Eur. Phys. J. Spec. Top.
https://doi.org/10.1140/epjs/s11734-021-00320-9

THE EUROPEAN PHYSICAL JOURNAL SPECIAL TOPICS

Regular Article

A new data-hiding algorithm for multi-channel biomedical signals based on variable-order fractional chaotic neural networks with frequency effect

Sezgin Kaçar[a]

Electrical and Electronics Engineering Department, Sakarya University of Applied Sciences, Sakarya, Turkey

Received 23 June 2021 / Accepted 25 October 2021

Abstract In this study, a new variable-order fractional chaotic neural network with frequency effect is proposed based on Hopfield Neural Network Under Electromagnetic Radiation, which is used to model brain functions in the literature. The numerical solution of this proposed system is carried out by the Grünwald–Letnikov (G–L) method, and time series and phase portraits are presented. In addition, the chaotic behavior is analyzed by Lyapunov exponent analysis according to the frequency parameter used for the variable-order function. A Pseudo-Random Number Generator (PRNG) is designed for data security applications using the obtained state variables and the usability of the PRNG is demonstrated with the NIST-800-22 test. Afterward, a data-hiding algorithm for personal data is presented for multi-channel biomedical signals based on the designed PRNG. With this algorithm, implementations are made for EEG, ECG, and EMG signals. It is shown in time and frequency domains that the method is usable for data-hiding applications. In addition, the effectiveness of the newly developed algorithm is proven with statistical methods.

1 Introduction

In recent years, as a result of the development of technology, chaotic systems have started to be used quite frequently in fields such as communication, data security, mechatronics, image processing, and physics [1–8]. In particular, random number generators (RNG), encryption, and data-hiding applications are the most prominent areas where chaotic features are used [9–25]. Chaotic systems are widely preferred in these applications because the obtained chaotic signals or state variables are randomly changing, unpredictable, and non-periodic.

The mathematical models of chaotic systems vary to the structure of the system parameters, their dimensions, the structure of their derivative orders, and their classes of discrete or continuous-time systems. Recently, continuous-time chaotic systems according to their derivative orders have been a trending subject of studies as a field of study and application. Derivative orders in chaotic systems are usually defined as integers. However, fractional-order chaotic systems with better nonlinear properties are widely available in the literature [26–31]. The most up-to-date trend in these matters is the study of variable-order systems beyond fractional-order systems [32,33].

Mathematical models defined as chaotic neural networks that show chaotic behavior are another widely studied topic today [34–37]. Chaotic neural networks can also be studied as integer order or fractional order [38–45]. One of the leading neural networks studied in the literature is the Hopfield Neural Network (HNN), used to model brain behaviors. The HNN model shows some behaviors such as periodic chaos, hyperchaos, and quasi period, which are quite complex. These behaviors increase even more under disturbances such as logic-pulse stimulates and electromagnetic radiations [46–48]. Therefore, this study prefers Hopfield Neural Network Under Electromagnetic Radiation (HNNUER) for PRNG design and personal data-hiding applications.

Studies on subjects such as data and information processing/storage, image encryption, synchronization, DSP and FPGA design, associative memory, and brain work patterns, which are based on integer and fractional-order HNN, are included in the literature [46–53]. However, there are very few studies using the HNNUER system as fractional order [49]. There is no work published as variable order for HNNUER. In this article, a study based on variable order for HNNUER is presented.

Data security applications can be made for biomedical signals or biomedical images using chaotic systems or chaotic neural networks [54–68]. However, when the literature is examined, it is seen that data security application is carried out for signals such as EEG,

[a] e-mail: skacar@subu.edu.tr (corresponding author)

EMG, ECG, which are recorded as multi-channel, with a single signal belonging to a single channel every time. In this study, a new algorithm for multi-channel biomedical signals is presented for the first time in the literature, more suitable for real applications.

Considering all these explanations, the contribution of the presented study to the literature can be summarized as follows. In this article, a new Variable-order Fractional Chaotic Neural Networks With Frequency Effect (VFCNNWFE) based on HNNUER is presented for the first time in the literature. In this new system, for the first time in the literature, the frequency parameter is added to the time-dependent function used to create a variable-order fractional. Numerical solution for VFCNNWFE is realized by Grünwald–Letnikov (G–L) method. Time series and phase portraits were obtained with the state variables calculated by the G–L method. In addition, Lyapunov exponent analysis was performed for the newly added frequency parameter, and it was proven that VFCNNWFE showed chaotic behavior. To demonstrate the usability of the presented system in data security applications, a new Pseudo-Random Number Generator (PRNG) was designed using state variables obtained from the VFCNNWFE system. Based on this PRNG, for the first time in the literature, a new data-hiding algorithm has been developed that hides 2 Kbits of personal data into multi-channel biomedical signals.

The paper has been planned as follows: VFCNNWFE and numerical results are presented in Sect. 2; PRNG design based on VFCNNWFE is given in Sect. 3; the new data-hiding algorithm is presented in Sect. 4, simulation results for multi-channel EMG, EEG, and ECG signals have given in Sect. 5 and conclusions are given in Sect. 6.

2 Mathematical model of VFCNNWFE

The mathematical model of the Variable-Order Fractional Chaotic Neural Network With Frequency Effect (VFCNNWFE) proposed in this study is given in Eq. (1). Equation (1) is the mathematical model, which was revised as variable order and a frequency parameter added to the variable-order function, based on fractional-order Hopfield Neural Network Under Electromagnetic Radiation which is defined in the literature [49]:

$$\begin{aligned} D^{q(\omega t)}x_1(t) &= -x_1(t) + a\tanh(x_1(t)) + b\tanh(x_2(t)) \\ &\quad + c\tanh(x_3(t)) \\ D^{q(\omega t)}x_2(t) &= -x_2(t) - d\tanh(x_1(t)) + e\tanh(x_2(t))... \\ &\quad ... - f\tanh(x_3(t)) - gx_2(t)\left(h - kx_4(t)^4\right) \\ D^{q(\omega t)}x_3(t) &= -x_3(t) + m\tanh(x_1(t)) - p\tanh(x_2(t)) \\ &\quad + r\tanh(x_3(t)) \\ D^{q(\omega t)}x_4(t) &= u1x_2(t) - wx_4(t). \end{aligned} \tag{1}$$

Parameter values determined for VFCNNWFE in Eq. (1) are given as a = 1.5, b = 2, c = 0.9, d = 1.5, e = 1.5, f = 0.45, g = 0.43, h = 1.519, k = 0.12, m = 3, p = 2, r = 1.5, u = 1.5, v = 0.1 and w = 0.45. The q(ωt) seen in Eq. (1) defines a variable-order fractional function with frequency parameter and is given in Eq. (2):

$$q(\omega t) = q_0 + \alpha\cos(\omega t) + \beta\sin(\omega t). \tag{2}$$

The parameter values seen in Eq. (2) are determined as q_0=0.96, α=0.025, β=0.025 and ω=1.5 rad/s. According to the parameters in Eq. (2), the fractional-order value of VFCNNWFE varies between q_{min}= 0.9246 and q_{max}=0.9954. This range of values is quite large compared to similar studies in the literature. A large range increases the dynamic properties of the proposed system. When the initial values of the state variables are determined as $x_1(0) = 0.1$, $x_2(0)$=− 0.1e, $x_3(0)$=0.1 and $x_4(0)$=− 0.1e together with the system parameter values given above, the system shows chaotic behavior. Numerical calculation for the proposed VFCNNWFE was performed using the G–L method [51,69–73] as seen in Eq. (3):

$$\begin{aligned} &{}^{G-L}D_x^v\, \mathrm{s}(x) \\ &= \lim_{N\to\infty}\left\{\frac{\left(\frac{x-a}{N}\right)}{\Gamma(-v)}\sum_{k=0}^{N-1}\frac{\Gamma(k-v)}{\Gamma(k+1)}s\left(x - k\left(\frac{x-a}{N}\right)\right)\right\}. \end{aligned} \tag{3}$$

In the definition of G–L seen in Eq. (3), s(x) is the differintegrable function, (a,x) is the start and end duration of the s(x) function, v is fractional-order, Γ is Gamma function. ${}^{G-L}D_x^v$ defines Grünwald–Letnikov fractional differential operator.

The time series and phase portraits of the obtained state variables from the proposed VFCNNWFE, which is calculated with the G–L method for the specified parameters and initials, are presented in Figs. 1 and 2. When Fig. 1 is examined, it is seen that the time series of the VFCNNWFE change randomly and are nonperiodic. In Fig. 2, the resulting phase portraits can evaluate as multiple attractors and they have chaotic trajectories. The results in Figs. 1 and 2 show that the VFCNNWFE proposed in Eq. (1) can be considered as a chaotic system.

In addition, Lyapunov exponents' analysis was also carried out to show that the system is chaotic and to demonstrate the effect of the newly added frequency parameter (ω) on the chaos behavior. The analysis results obtained are shown in Fig. 3. When Fig. 3 is examined, it can be seen that the VFCNNWFE system exhibits chaotic behavior between nearly $\omega = 0$ and 2 rad/s. Between nearly $\omega = 2$ and 4 rad/s, sometimes it is chaotic and sometimes it is not chaotic. After $\omega = 4$ rad/s, it is not chaotic and it appears to be completely out of chaos. Accordingly, it has been shown that the system exhibits chaotic behavior for the $\omega = 1.5$ rad/s value determined in Eq. 2.

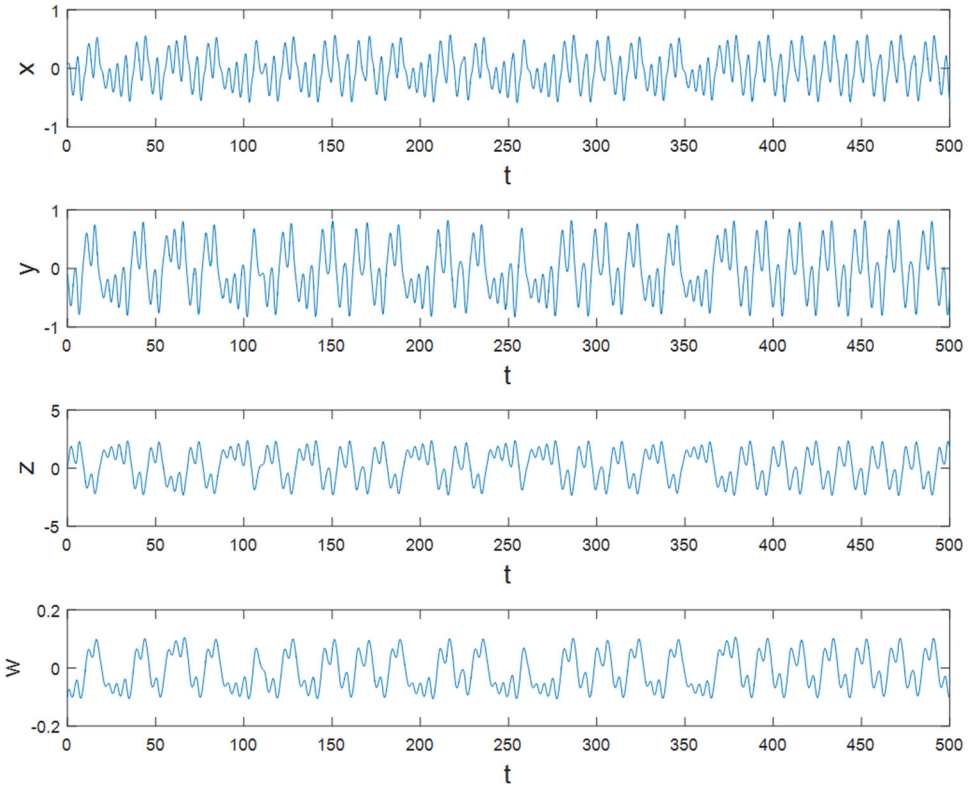

Fig. 1 Time series of state variables of VFCNNWFE

3 VFCNNWFE-based PRNG design

In this section, a new PRNG designed based on the state variables obtained from the numerical solution of the VFCNNWFE system is introduced. The most important factor is that the chaotic system used in data security applications such as chaos-based encryption and data hiding has sufficient randomness. With this PRNG design, it is aimed to show that the proposed system has sufficient randomness.

Figure 6 shows the flow diagram of the designed PRNG. In the PRNG design, as a first step, the parameters and initial values of the VFCNNWFE system are determined. Afterward, numerical results are obtained with the G–L method. Each calculated state variable is converted to binary format in each iteration. 9 LSB bits of each state variable are taken and a 36-bit bit array is formed in each iteration. These iterations continued until there are 1000000 bits in total. When the array of 1000000 bits required by the NIST-800-22 test is completed, the NIST-800-22 test is performed using NIST Statistical Test Suit Software (sts-2.1.1) [74].

The NIST-800-22 test includes 15 different statistical tests (seen in Table 1) for determining the randomness of bit arrays. For all of these tests, the results about randomness are presented using P values. If the calculated P value for one of the tests is obtained equal to 1, this means the bit array has perfect randomness. If the obtained P value is equal to zero, this means the bit array is not random. On the other hand, for P value $\geq$ 0.001 situations, the bit array can be considered to be random with a confidence of 99.9% [75]. For this reason, if the calculated P values for the NIST tests are between 0.001 and 1, the tested bit array is accepted as random in the literature. The performed NIST test results for the developed PRNG are presented in Table 1. When the results in Table 1 are examined, it is seen that all results (P values) are between 0.001 and 1, which is the success criteria of the test. According to these results, it has been shown that VFCNNWFE-based PRNG has sufficient randomness.

4 The new data-hiding algorithm for multi-channel biomedical signals

In this section, the new data-hiding algorithm for multi-channel biomedical signals, developed based on the PRNG designed in the previous section, is presented (in Fig. 7). In the developed data-hiding algorithm, personal data to be hidden are hidden in multi-channel biomedical signals. Accordingly, personal data are message data, and the used multi-channel biomedical signals are carrier signals.

The data-hiding algorithm seen in Fig. 7 is performed for each bit of message (personal) data. State variables (x1, x2, x3 and x4) calculated with the G–L method in each iteration are converted to binary format for each personal data bit that is desired to be hidden. Then, in accordance with the PRNG, 9 bits are taken from each state variable and a 36-bit binary array is created. The last 4 bits of this array are used to determine which

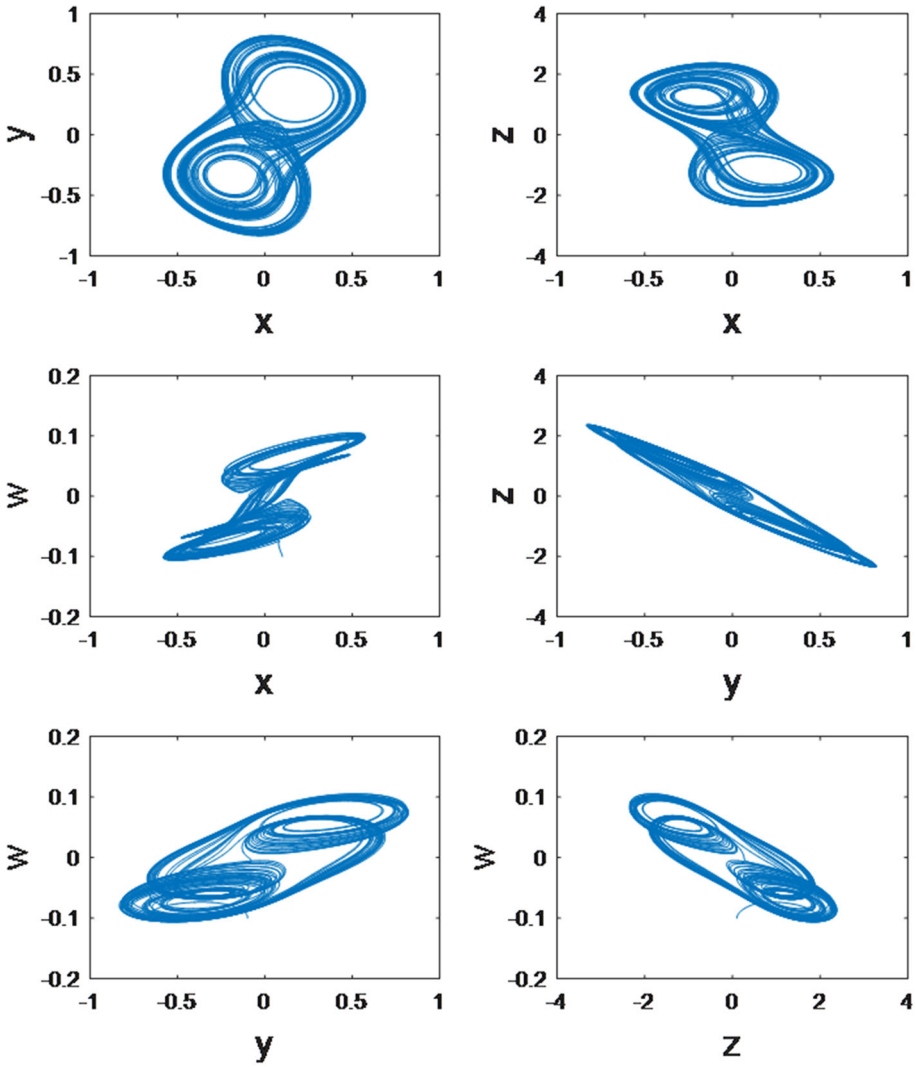

Fig. 2 Phase portraits of state variables of VFCNNWFE

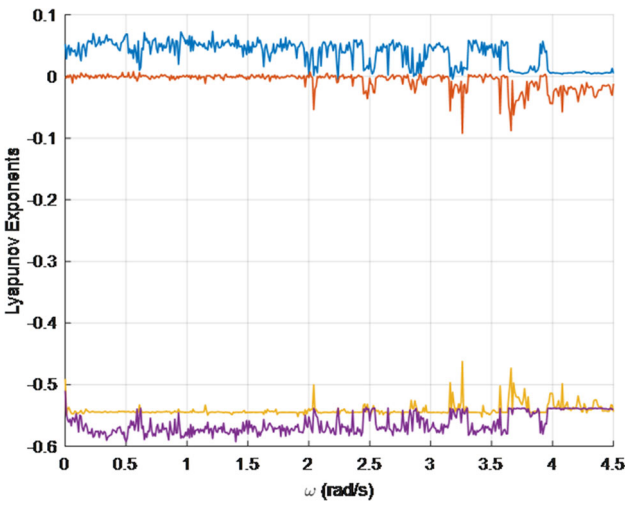

Fig. 3 Lyapunov exponents of VFCNNWFE for ω parameter

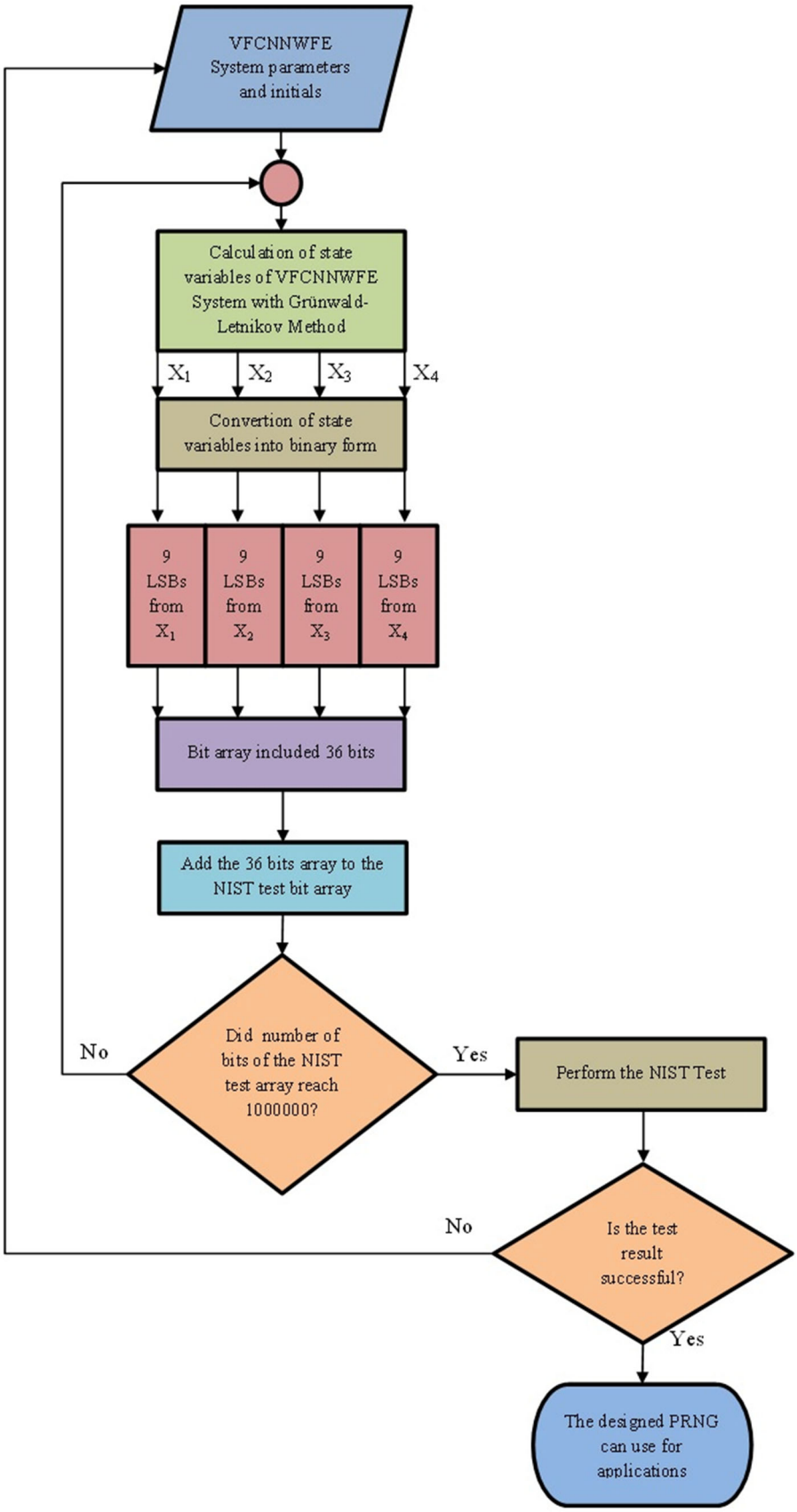

Fig. 4 Flowchart of the designed PRNG

Table 1 NIST-800-22 test results of VFCNNWFE-based PRNG

Statistical tests	P value	Result
Frequency (Monobit) test	0.683273674902085	Successful
Block-frequency test	0.459958782937705	Successful
Cumulative-sums test	0.889834169201796	Successful
Runs test	0.765576078258594	Successful
Longest-run test	0.46087909724265	Successful
Binary matrix rank test	0.726827620827944	Successful
Discrete Fourier transform test	0.251349108810223	Successful
Non-overlapping templates test	0.0044831701237676	Successful
Overlapping templates test	0.813034059559583	Successful
Maurer's universal statistical test	0.0239984428650677	Successful
Approximate entropy test	0.576435276890138	Successful
Random-excursions test ($x = -4$)	0.373733486465795	Successful
Random-excursions variant test ($x = -9$)	0.0924883183589073	Successful
Serial Test-1	0.42790111377448	Successful
Serial Test-2	0.201530218143745	Successful
Linear-complexity test	0.258401444956329	Successful

channel of the multi-channel biomedical signals is used to hide data. With the remaining 32 bits, it is determined which value of the selected channel is used to hide data. By the performed control in the algorithm, a used carrier data cannot be used later. In this way, a unique carrier value is determined for each personal data bit. Thus, no data loss occurs. Data hiding is performed by placing the personal data bit on the LSB of the determined carrier value. With this algorithm, any data hiding can be done into multi-channel biomedical signals such as EEG, ECG, and EMG. After the data-hiding process is completed, the reverse of the processes in the developed algorithm is performed to retrieve the hidden data.

5 Simulation results for multi-channel EMG, EEG, and ECG signals

In this section, simulation and analysis results of the newly developed data-hiding algorithm for EMG, EEG, and ECG signals with different channel numbers and data lengths are presented. First of all, time series, histogram distributions, and frequency spectrums of original and data-hidden EMG, EEG, and ECG signals are presented. Afterward, entropy, mean, standard deviation, correlation, SSIM (Structural Similarity Index), PSNR, and MSE results obtained for all signals are given together, and the effectiveness of the algorithm on different signals is examined.

Considering the number of channels and data lengths for all used signals, the total number of data was determined as 77,128. In this way, the LSB data-hiding capacity of all used signals is equalized. Thus, the performance evaluations became more meaningful with the equal number of data used in the signals. Personal data consisting of 256 characters and a length of 2048 bits (2 Kbits) have been hidden in all used signals. The hidden text is shown below. This text has been successfully recovered, fully and sequentially, after successful hiding to all signals. This shows that the developed algorithm works correctly.

Text of the hidden personnel data:
"Name: Sezgin; Surname: Kaçar; ID: 0123456789; Date of Birth: 1.1.XXXX; Place of Birth: XXXXX, Turkey; Phone no: +90123456789; Address: Sakarya University of Applied Sciences, Faculty of Technology, Department of Electrical and Electronics Engineering, Turkey".

5.1 Simulation results

In this section, the used multi-channel biomedical signals have been regulated as follows: the EMG data recorded over 8 channels that contain 9641 values in each channel, the EEG data recorded over 14 channels that contain 5509 values in each channel, and the ECG data received over 6 channels that contain 12,855 values in each channel. After the data regulation, the developed data-hiding algorithm has been applied. For each channel of each signal, original and data-hidden time series, histogram distributions, and frequency spectrums have been obtained. But, when the all obtained results of all channels are presented graphically, there are a lot of figures which make it difficult to follow the paper. So that, some of the selected channels are presented here. The used original EMG signals and the data-hidden EMG signals are shown in Fig. 6 for channels 1, 5, and 8; the used original EEG signals and the data-hidden EEG signals are shown in Fig. 7 for channels 1, 5, 9, and 14; the used original ECG signals and the data-hidden ECG signals are shown in Fig. 8 for channels 1 and 5. When Figs. 6, 7, and 8 are examined, it is seen that there is no difference between the original and data-hidden signals. Accordingly, as a result of the visual analysis, it was seen that the data-hiding application was successful.

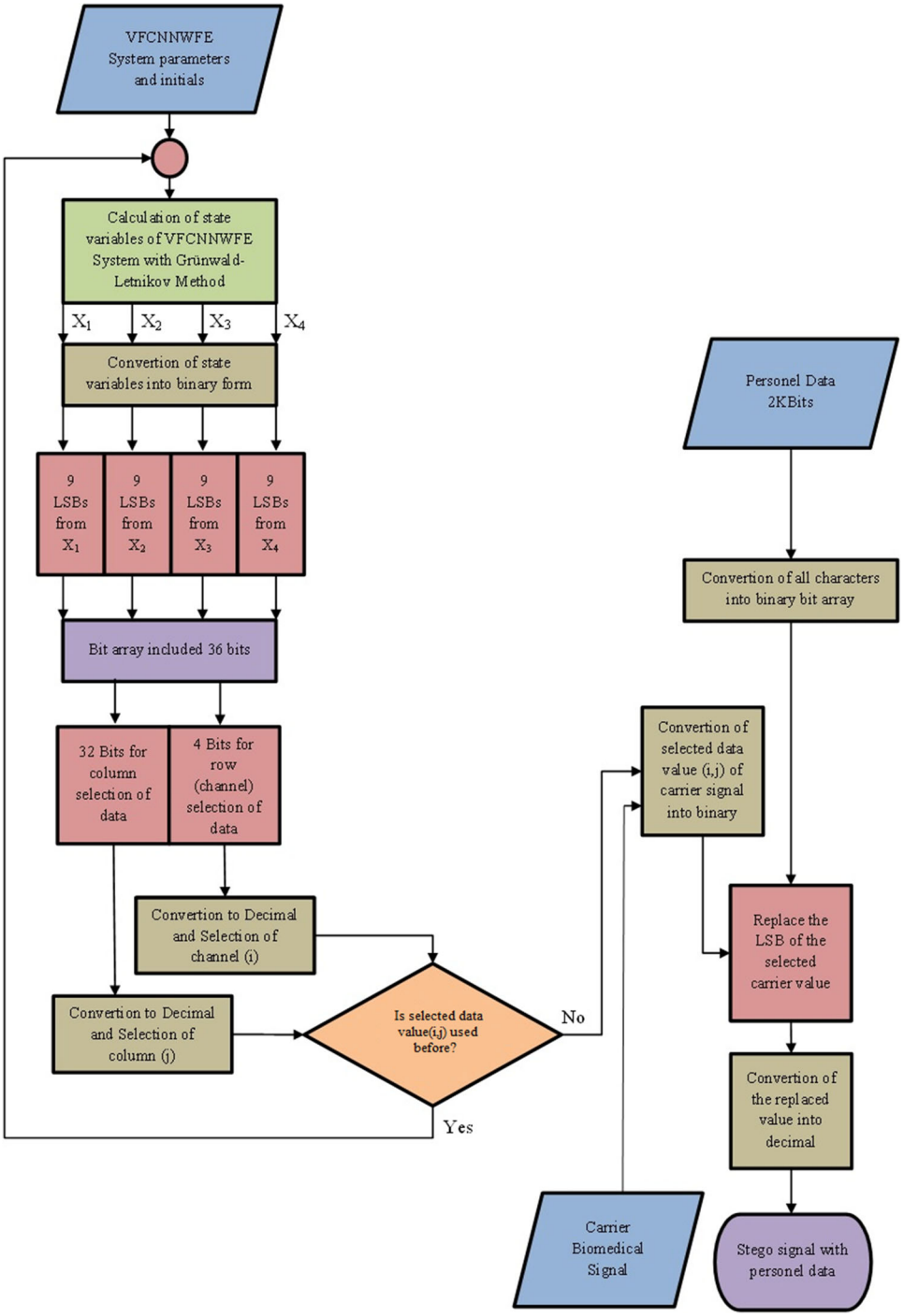

Fig. 5 Flowchart of data-hiding algorithm

After the time series of the signals, the histogram distributions have been analyzed to see if the data hiding changed the distribution of the values of the signals. Figure 9 shows histograms of the used original EMG signals and the data-hidden EMG signals for channels 1, 5, and 8. Histograms of the used original EEG signals and the data-hidden EEG signals are shown in Fig. 10 for channels 1, 5, 9, and 14. Figure 11 shows the histograms of the used original ECG signals and the data-hidden ECG signals for channels 1 and 5.

When Figs. 9, 10, and 11 are examined, it is seen that there is no difference between the histograms obtained for the original and data-hidden signals. These results show that the data-hiding application does not negatively affect the value distribution in biomedical signals, which are the carrier data, and does not change the distribution. Accordingly, as a result of the histogram analysis, it was seen that the data-hiding application was successful.

Another analysis performed on the original and the data-hidden signals are frequency spectrum analysis

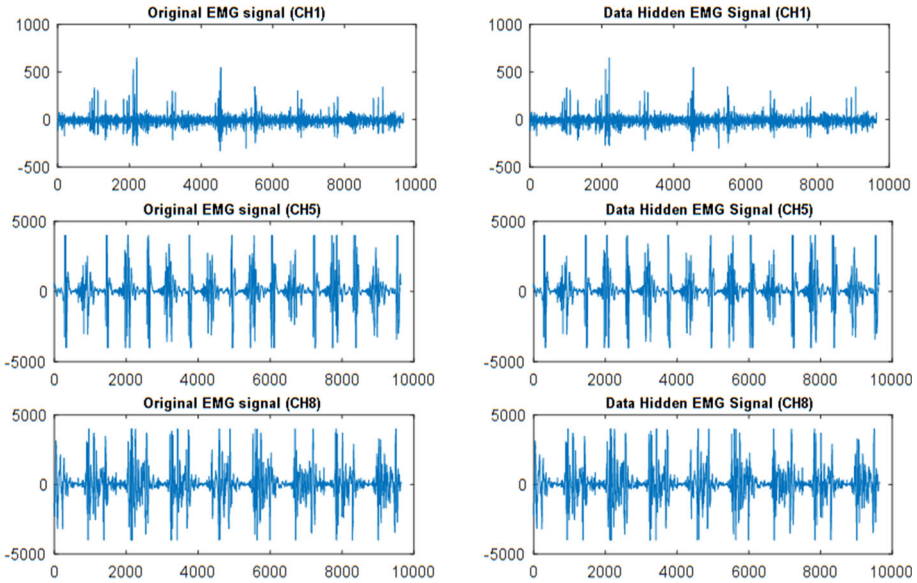

Fig. 6 Original and steno signals of EMG data for channels 1, 5, and 8

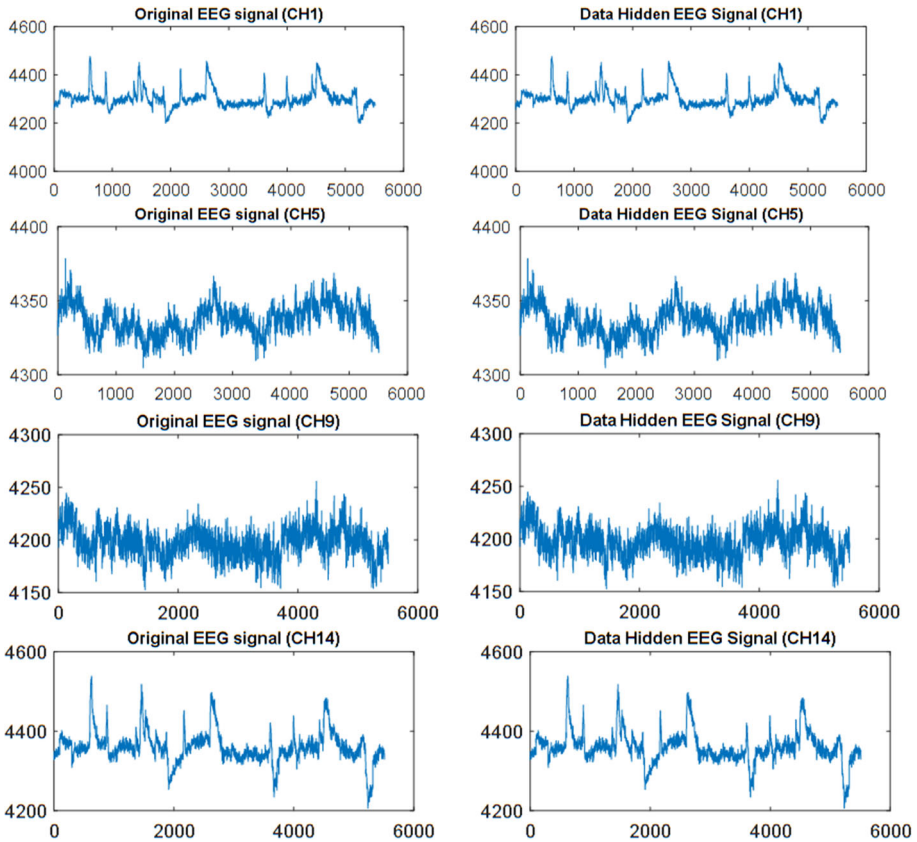

Fig. 7 Original and steno signals of EEG data for channels 1, 5, 9, and 14

with FFT. Figure 12 shows frequency spectrums of the used original EMG signals and the data-hidden EMG signals for channels 1, 5, and 8. Frequency spectrums of the used original EEG signals and the data-hidden EEG signals are shown in Fig. 13 for channels 1, 5, 9, and 14. Figure 14 shows frequency spectrums of the used original ECG signals and the data-hidden ECG signals for channels 1 and 5.

When Figs. 12, 13, and 14 are examined, it is seen that there is no difference between the frequency spectrums obtained for the original and data-hidden signals. These results show that the data-hiding application does not adversely affect the frequency components in the used biomedical signals and there is no data loss. Accordingly, as a result of the frequency spectrum analysis, data hiding was found to be successful.

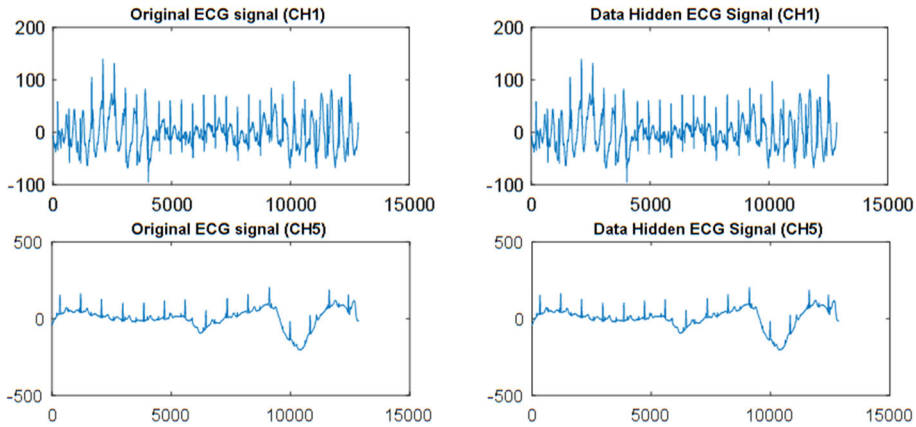

Fig. 8 Original and steno signals of ECG data for channels 1 and 5

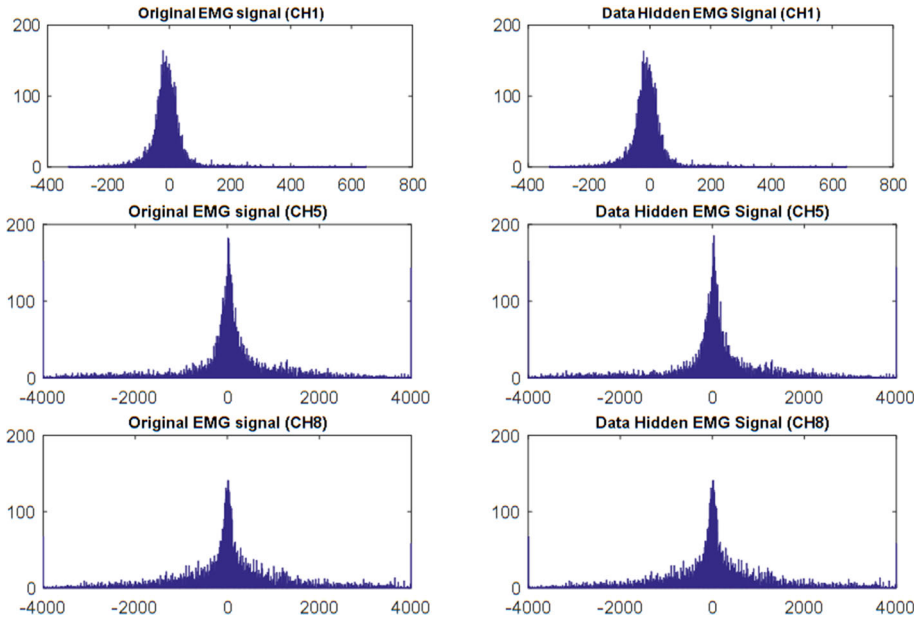

Fig. 9 Histogram distributions of original and steno signals of EMG data for channels 1, 5, and 8

The last analyses as presented visually are the plots of different values of steno signals and the original signals, in Figs. 15, 16, and 17 for EMG, EEG, and ECG signals, respectively. In these figures, the different values of steno signals obtained after LSB data hiding are seen on the original EMG, EEG, and ECG signals.

When Figs. 15, 16, and 17 are examined, all the different values of steno signals obtained after LSB data-hiding processes are seen overlapped with the originals signals of EMG, EEG, and ECG signals and there is no deviation on the steno signals values. These results show that the data-hiding processes do not cause any deformation on the original signals.

All the obtained results showed that the application of data hiding did not cause a significant change on different biomedical signals, which are carrier data. This situation also shows that diagnosis can be made via data-hidden signals. In this way, the developed application is seen as usable in real life.

5.2 Statistical analysis results

In this section, entropy, mean, standard deviation, correlation, SSIM (Structural Similarity Index), PSNR, and MSE results are obtained to demonstrate the effectiveness of data hiding and confirm the simulation results. Entropy (in Eq. (4)) provides information about the randomness of the signals:

$$H(s) = -\sum_{i=1}^{N} s(i) log_2(s(i)). \tag{4}$$

Mean is the average value of the signal. The formula of mean is given in Eq. 5:

$$E(x) = \frac{1}{N}\sum_{i=1}^{N} x_i. \tag{5}$$

The standard deviation is a metric of the amount of variation of values of a signal. It can be seen in Eq. 6:

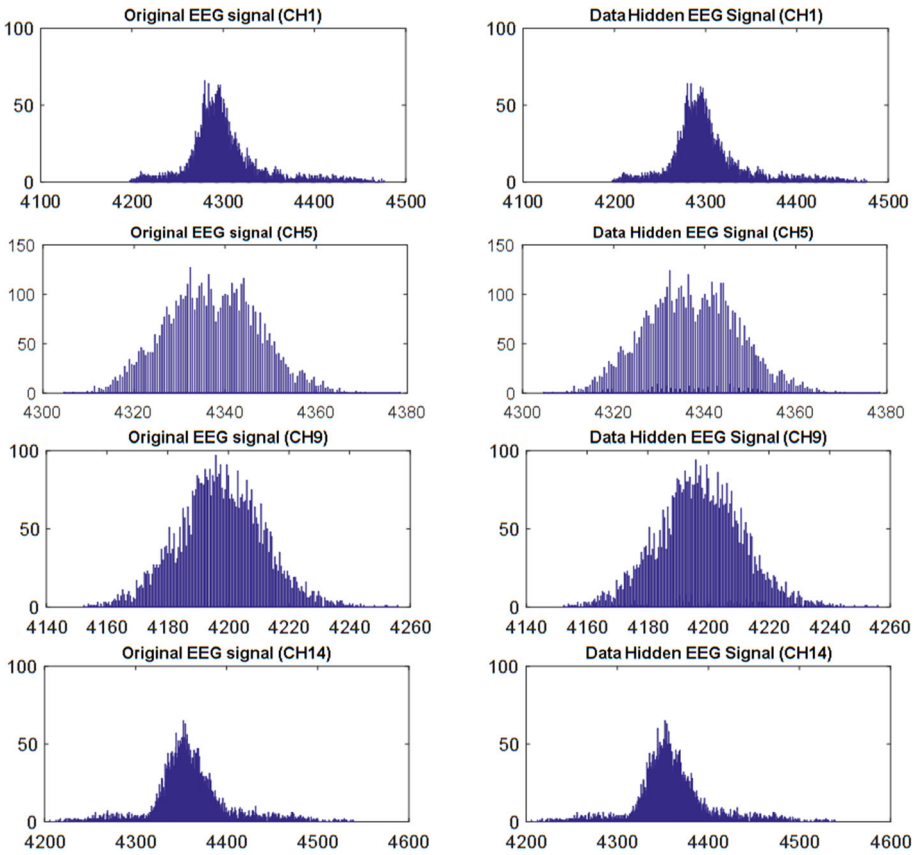

Fig. 10 Histogram distributions of original and steno signals of EEG data for channels 1, 5, 9, and 14

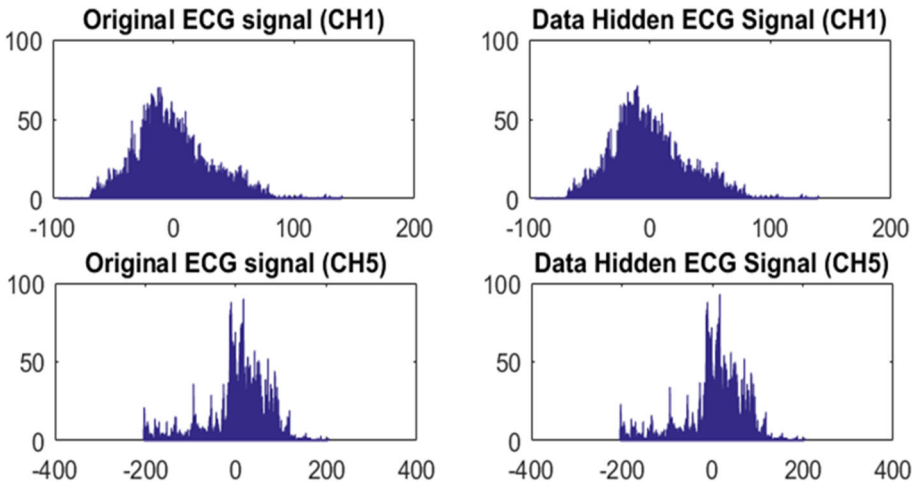

Fig. 11 Histogram distributions of original and steno signals of ECG data for channels 1 and 5

$$D(x) = \frac{1}{N}\sum_{i=1}^{N}(x_i - E(x))^2. \tag{6}$$

Another used statistical parameter is correlation which gives the similarity between two signals. The correlation value can be calculated with Eq. (7):

$$corr(x,y) = \frac{cov(x,y)}{\sqrt{D(x)D(y)}}. \tag{7}$$

In Eq. (7), cov(x,y) means covariance between two signals that can be calculated with Eq. (8):

$$cov(x,y) = \frac{1}{N}\sum_{i=1}^{N}(x_i - E(x))(y_i - E(y)). \tag{8}$$

In Eq. (9), the formula of SSIM is given. SSIM value is another similarity metric between two signals like correlation:

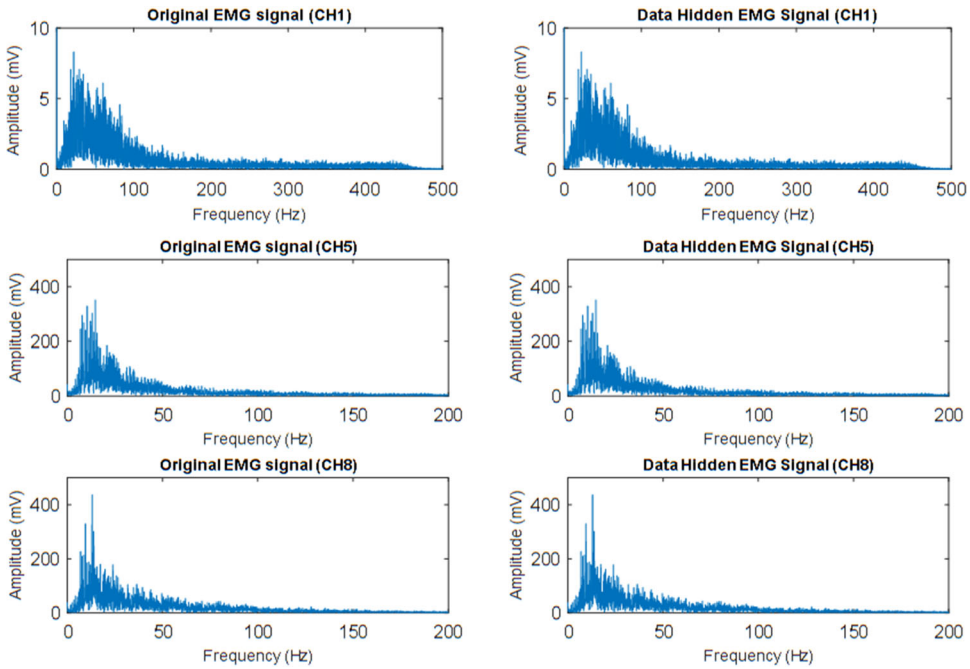

Fig. 12 Frequency spectrums of original and steno signals of EMG data for channels 1, 5 and 8

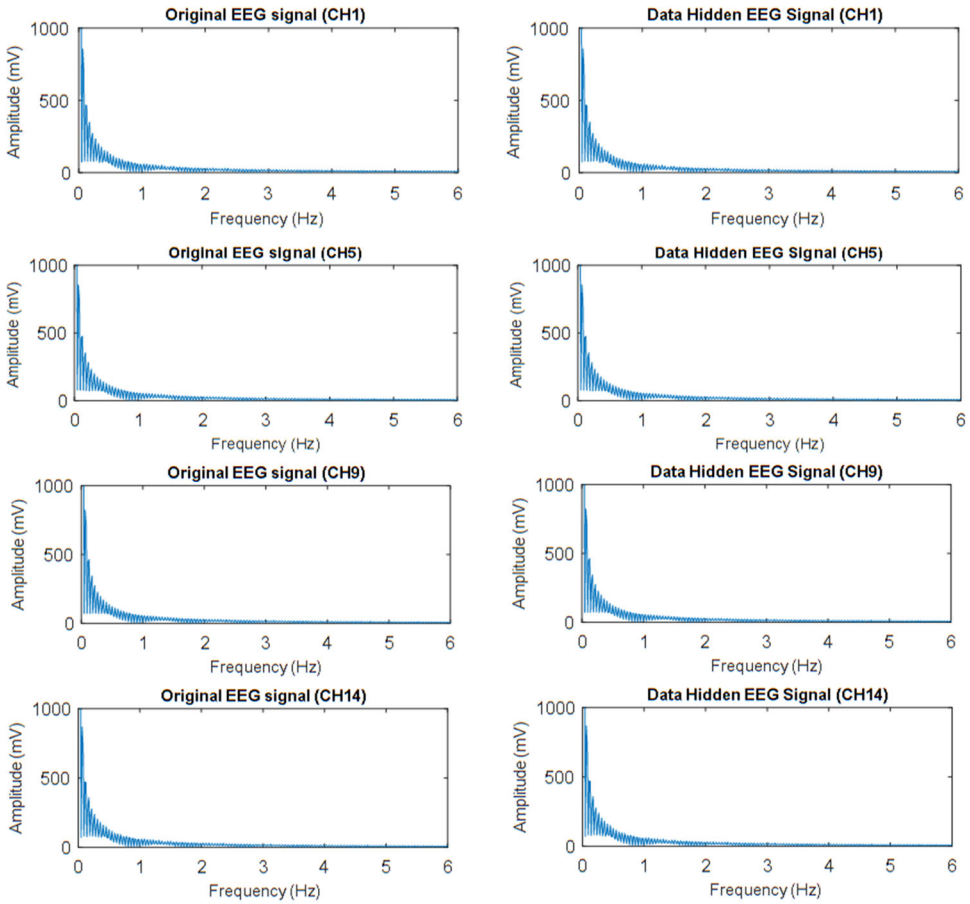

Fig. 13 Frequency spectrums of original and steno signals of EEG data for channels 1, 5, 9 and 14

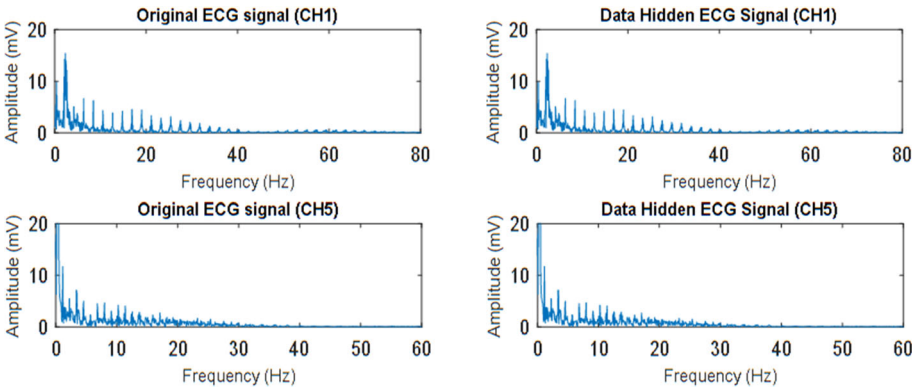

Fig. 14 Frequency spectrums of original and steno signals of ECG data for channels 1 and 5

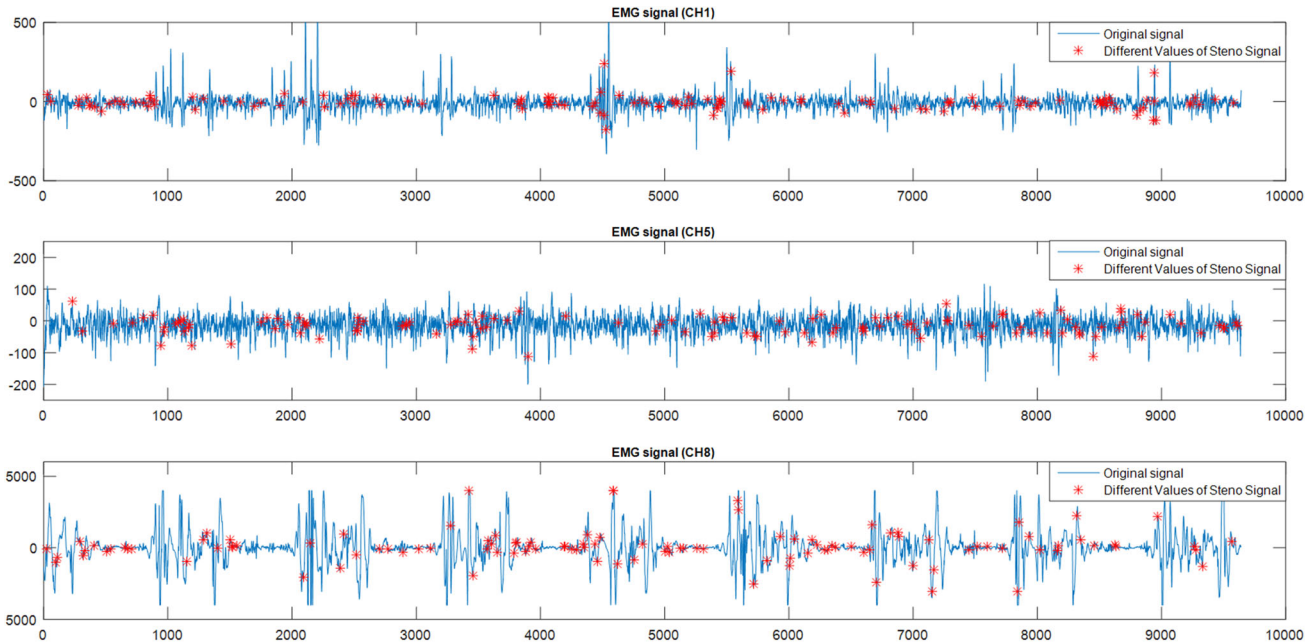

Fig. 15 Original EMG signals and different values of steno EMG signals after LSB data hiding for channels 1, 5, and 8

$$SSIM(x,y) = \frac{(2E(x)E(y)+C_1)(2cov(x,y)+C_2)}{(E(x)^2+E(y)^2+C_1)(D(x)^2+D(y)^2+C_2)}. \quad (9)$$

The formulas of PSNR and MSE which are used commonly in literature for comparing two signals are given in Eqs. (10) and (11):

$$PSNR = 10log_{10}\frac{MAX(x)^2}{MSE} \quad (10)$$

$$MSE = \frac{1}{N}\sum_{i=1}^{N}(x_i - y_i)^2. \quad (11)$$

The obtained results are given in Table 2 comparatively. When these results are examined, it is seen that the entropy, mean, and standard deviation values are very close or the same to each other in the original and data-hidden steno signals for all signal types (EMG, EEG, and ECG). When these values are very close or the same for the original and the steno signals, this means the signals are similar to each other. In addition, the obtained correlation and SSIM values for original and steno signals are almost equal to 1 which means the original and steno signals are nearly the same for EMG, EEG, and ECG signals. These results show that the data-hiding application does not cause a statistically significant change in the signals. PSNR and MSE values in Table 2 also reveal the similarity between original and steno signals in all signal types. Accordingly, the obtained PSNR values show that the original signals do not deteriorate much in data-hiding applications, while the MSE values show that the differences between the original signals and the steno signals are negligible. All these results show that the data-hiding application is quite successful and effective, but also confirms the obtained simulation results.

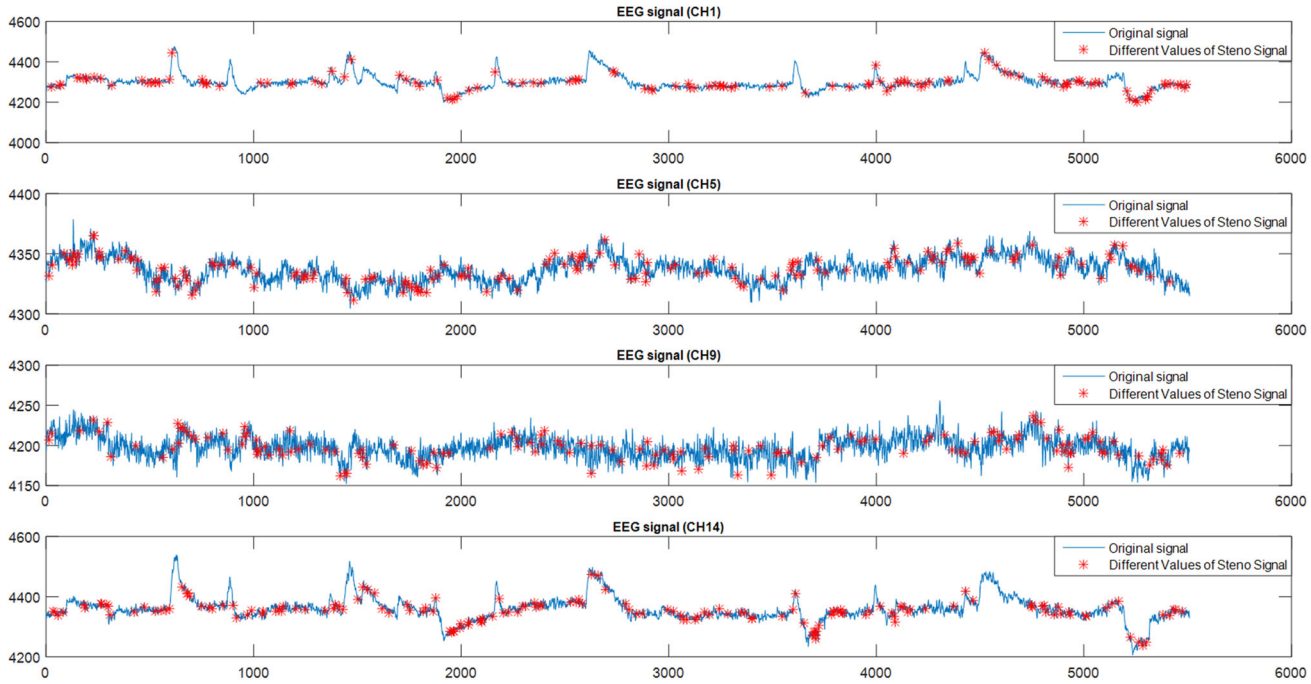

Fig. 16 Original EEG signals and different values of steno EEG signals after LSB data hiding for channels 1, 5, 9, and 14

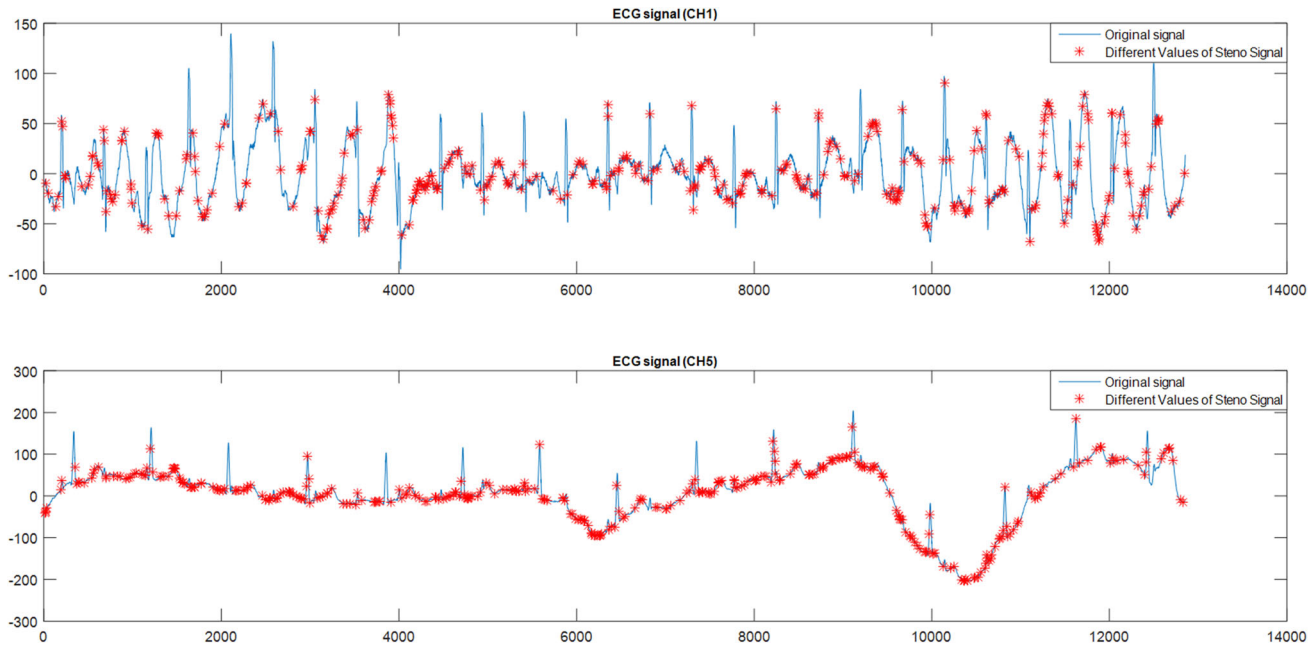

Fig. 17 Original ECG signals and different values of steno ECG signals after LSB data hiding for channels 1 and 5

6 Conclusions

In this study, for the first time in the literature, a chaotic neural network with frequency parameter in variable-order function has been presented and it has been proved that it exhibits chaos behavior by successfully performing the analysis. Thus, a new parameter has been introduced for variable-order systems in the literature. A new PRNG design was made using the dynamic features of the proposed system and successful results were obtained. Based on the designed PRNG, data hiding has been implemented for the first time in the literature for multi-channel biomedical signals, including EMG, EEG, and ECG. A new algorithm has been developed for this application. With the developed algorithm, successful simulation and analysis results were obtained for multi-channel EMG, EEG, and ECG signals, and the effectiveness of the developed

Table 2 Statistical results for multi-channel biomedical signals

	EMG		EEG		**ECG**	
	Original	Steno	Original	Steno	Original	Steno
Entropy	9.6161	9.6241	9.7498	9.8887	9.9494	10.0448
Mean	13.3214	13.3233	4.2992	4.2992	4.2109	4.2276
Stand. dev.	9.1765	9.1765	3.5351	3.5350	2.5564	2.5562
Correlation	0.9999		0.9999		0.9999	
SSIM	0.9998		0.9999		0.9986	
PSNR	66.8326		64.4587		63.8260	
MSE	0.0135		0.0233		0.0269	

algorithm was demonstrated. Although 2.66% (2 Kbits) of the data amount of biomedical signals are hidden, the results obtained are quite good. For example, according to all comparative graphics in time and frequency domains and histograms in Figs. 6, 7, 8, 9, 10, 11, 12, 13 and 14, there are no differences between the original and steno signals. In addition, it is shown in Figs. 15, 16 and 17 that the different values of steno signals do not affect the structure of the original signals. In addition, the statistical results in Table 2 show that the original and steno signals are nearly the same. Accordingly, it can be said that the proposed algorithm for multi-channel signals increases the data-hiding capacity and does not cause a significant deterioration in biomedical signals.

References

1. L. Jiancheng, K. Rajagopal, L. Tengfei, S. Kaçar, B. Arıcıoğlu, Ü. Çavuşoğlu, A.H. Kökçam, A. Karthikeyan, Math. Probl. Eng. **2020**, 8083509 (2020)
2. S. Kacar, Z. Wei, A. Akgul, B. Aricioglu, Zeitschrift für Naturforschung A **73**, 7 (2018)
3. Ü. Çavuşoğlu, Y. Uyaroğlu, Pehlivan J. Fac. Eng. Archit. Gaz. **29**, 1 (2014)
4. C. Li, İ Pehlivan, J.C. Sprott, Turk. J. Electr. Eng. Co. **24**, 1 (2016)
5. M. Cimen, Z. Garip, M. Pala, A.F. Boz, A. Akgül, Chaos Theory Appl. **1**, 1 (2019)
6. Ü. Çavuşoğlu, A. Zengin, İ Pehlivan, S. Kaçar, Nonlinear Dyn. **87**(2017)
7. E. Pehlivan, Q. Kurt, A. Lai, M. Basaran, Kutlu. Chaos Theory Appl. **1**, 1 (2019)
8. Y. Adıyaman, S. Emiroglu, M. Uğar, M. Yıldız, Chaos Theory Appl. **2**, 1 (2020)
9. S. Kaçar, Optik **127**, 20 (2016)
10. A. Akgül, S. Kaçar, B. Aricioğlu, İ . Pehlivan, in Proceedings of IEEE 8th International Conference On Electrical And Electronics Engineering [ELECO], Bursa/ TURKEY (2013)
11. Ü. Çavuşoğlu, A. Akgul, A. Zengin, Pehlivan. Chaos Solitons Fractals **104**(2017)
12. B. Gürevin, M. Yıldız, E. Güleryüz, M. Kutlu, Ö. Sorgun, Chaos Theory Appl. **2**, 2 (2020)
13. A. Akgul, M.Z. Yildiz, O.F. Boyraz, E. Guleryuz, S. Kacar, B. Gurevin, J. Fac. Eng. Archit. Gaz. **35**, 3 (2020)
14. L. Moysis, A. Tutueva, C. Volos, D. Butusov, Chaos Theory Appl. **2**, 2 (2020)
15. S. Vaidyanathan, A. Akgul, S. Kaçar, U. Cavusoğlu, Eur. Phys. J. Plus **133**, 46 (2018)
16. A. Arshad, S. Shaukat, A. Ali, A. Eleyan, S. Shah, J. Ahmad, Chaos Theory Appl. **2**, 1 (2020)
17. A. Akgul, S. Kacar, B. Aricioglu, Nonlinear Dyn **90**(2017)
18. M. Alçın, Chaos Theory Appl. **2**, 1 (2020)
19. C. Bayilmis, Ü. Çavuşoğlu, A. Akgul, S. Kacar, A. Sevin, Tehnicki Vjesnik. **24**(2017)
20. S. Vaidyanathan, A. Akgul, S. Kaçar, U. Cavusoğlu, Eur. Phys. J. Plus **133**, 46 (2018)
21. C. Bayilmis, Ü. Çavuşoğlu, A. Akgul, A. Sevin, S. Kacar, in *Proceedings of International Conference on Computer Science and Information Systems, Dubai, (2014)*, p. 89
22. S. Agarwal, Chaos Theory Appl. **3**, 1 (2021)
23. Ü. Çavuşoğlu, S. Kaçar, I. Pehlivan, A. Zengin, Chaos Solitons Fractals **95**(2017)
24. M. Alçın, M. Tuna, P. Erdoğmuş, Koyuncu. Chaos Theory Appl. **3**, 1 (2021)
25. Ü. Çavuşoğlu, A. Akgul S. Kaçar, I. Pehlivan, A. Zengin, Security Comm. Networks **9**, (2016)
26. K. Rajagopal, A. Akgul, S. Jafari, B. Aricioglu, Nonlinear Dyn. **91**(2018)
27. H. Jahanshahi, A. Yousefpour, J.M. Munoz-Pacheco, S. Kacar, V.T. Pham, F.E. Alsaadi, Appl. Math. Comput. **383**, 125310 (2020)
28. J. Wang, L. Xiao, K. Rajagopal, A. Akgul, S. Cicek, B. Aricioglu, Symmetry **13**, 340 (2021)
29. H. Jahanshahi, J.M. Munoz-Pacheco, S. Bekiros, N.D. Alotaibi, Chaos Solit. Fract. **143**, 110632 (2021)
30. M. Çimen, Z. Garip, Ö. Boyraz, İ Pehlivan, M. Yıldız, A.F. Boz, Chaos Theory Appl. **2**, 1 (2020)
31. A. Akgül, C. Arslan, B. Arıcıoğlu, Chaos Theory Appl. **1**, 1 (2019)
32. J.F. Li, H. Jahanshahi, S. Kacar, Y.M. Chu, J.F. Gómez-Aguilar, N.D. Alotaibi, K.H. Alharbi, Chaos, Solitons Fractals **145**, 110681 (2021)
33. H. Jahanshahi, S.S. Sajjadi, S. Bekiros, A.A. Aly, Chaos Solit. Fract. **144**, 110698 (2021)
34. T. Li, A.G. Song, S.M. Fei, Y.Q. Guo, Nonlinear Anal. Theory Method. Appl. **71**(2009)
35. H. Jahanshahi, M. Shahriari-Kahkeshi, R. Alcaraz, X. Wang, V.P. Singh, V.-T. Pham, Entropy **21**, 156 (2019)

36. Q.T. Gan, R.X. Hu, Y.H. Liang, Commun. Nonlinear Sci. Numer. Simul. **17**(2012)
37. H. Lin, C. Wang, W. Yao, Y. Tan, Commun. Nonlinear Sci. Numer. Simul. **90**, 105390 (2020)
38. P. Arena, L. Fortuna, D. Porto, Phys. Rev. E **61**(2000)
39. P. Arena, R. Caponetto, L. Fortuna, D. Porto, Int. J. Bifurc. Chaos **8**(1998)
40. L.-L. Huang, J.H. Park, G.-C. Wu, Z.-W. Mo, J. Comput. Appl. Math. **370**, 112633 (2020)
41. X. Huang, Z. Zhao, Z. Wang, Y.X. Lia, Neurocomputing **94**(2012)
42. K. Moaddy, A.G. Radwan, K.N. Salama, S. Momani, I. Hashim, Comput. Math. Appl. **64**(2012)
43. Y.-L. Wang, H. Jahanshahi, S. Bekiros, F. Bezzina, Y.-M. Chu, A.A. Aly, Chaos Solit. Fract. **146**, 110881 (2021)
44. S. Zhou, H. Li, Z. Zhu, Chaos Solit. Fract. **36**(2008)
45. J. Yu, C. Hu, H. Jiang, Neural Netw. **35**(2012)
46. J. Yang, L. Wang, Y. Wang, T. Guo, Neurocomputing **227**(2017)
47. M.-F. Danca, N. Kuznetsov, Chaos Solitons Fractals **103**(2017)
48. K. Rajagopal, J.M. Munoz-Pacheco, V.T. Pham, D.V. Hoang, F.E. Alsaadi, F.E. Alsaadi, Eur. Phys. J. Spec. Top. **227**(2018)
49. F.M. Allehiany, E.E. Mahmoud, L.S. Jahanzaib, P. Trikha, H. Alotaibi, Results Phys. **21**, 103786 (2021)
50. A. Boroomand, M. Menhaj, in *Proceedings of International Conference on Neural Information Processing ICONIP 2008: Advances in Neuro-Information Processing, Auckland, 2009*, p. 883
51. Y. Pu, Z. Yi, J. Zhou, IEEE Trans. Neural Networks Learn. Syst. **28**, 10 (2017)
52. C. Ma, J. Mou, F. Yang, H. Yan, Eur. Phys. J. Plus **135**, 100 (2020)
53. L. Chen, J. Qu, Y. Chai, R. Wu, G. Qi, Entropy **15**(2013)
54. M.Z. Konyar, S. Öztürk, Symmetry **12**, 6 (2020)
55. M. Ahmad, O. Farooq, S. Datta, S.S. Sohail, A.L. Vyas, D. Mulvaney, *In Proceedings of 4th International Conference on Biomedical Engineering and Informatics (BMEI)* (China, Shanghai, 2011), p. 1471
56. F. Sufi, F. Han, I. Khalil, J. Hu, Secur. Commun. Netw. **4**, 5 (2011)
57. C.-F. Lin, C.-H. Chung, J.-H. Lin, Med. Biol. Eng. Comput. **47**, 7 (2009)
58. S. Thakur, A.K. Singh, S.P. Ghrera, M. Elhoseny, Multimed Tools Appl. **78**, 3 (2019)
59. C.-F. Lin, Int. J. Comp. Res. 18, **3/4** (2011)
60. C.-F. Lin, B.S.H. Wang, J. Mar. Sci. Technol. **19**, 6 (2011)
61. X. Hao, J. Wang, Q. Yang, X. Yan, P. Li, J. Med. Syst. **37**, 2 (2013)
62. S. Parveen, S. Parashar, Izharuddin, in *Proceedings of International Conference on Multimedia, Signal Processing and Communication Technologies, Aligarh, India 2011*, p. 68
63. A. Pandey, B.S. Saini, B. Singh, N. Sood, J. Med. Syst. **41**, 187 (2017)
64. R. Shahzadi, S.M. Anwar, F. Qamar, M. Ali, J.J.P.C. Rodrigues, M. Alnowami, IEEE Access **7**(2019)
65. T.-L. Liao, H.-C. Chen, C.-Y. Peng, Y.-Y. Hou, Electronics **10**, 359 (2021)
66. J.R. Mboupda Pone, S. Çiçek, S. Takougang Kingni, A. Tiedeu, M. Kom, Analog Integr Circ Sig Process **103**, (2020)
67. M.A. Murillo-Escobar, L. Cardoza-Avenda, R.M. Lopez-Gutierrez, C. Cruz-Hernandez, J. Med. Syst. **41**, 59 (2017)
68. A. Akgul, O.F. Boyraz, K. Rajagopal, E. Guleryuz, M.Z. Yildiz, M. Kutlu, Z. Naturforsch. **75**, 12a (2020)
69. K.B. Oldham, J. Spanier, *The Fractional Calculus: Theory and Applications of Differentiation and Integration to Arbitrary Order* (Academic, New York, 1974)
70. I. Podlubny, *Fractional Differential Equations: An Introduction to Fractional Derivatives, Fractional Differential Equations, to Methods of Their Solution and Some of Their Applications* (Academic, San Diego, 1998)
71. A.C. McBride, G.F. Roach, *Fractional Calculus* (Halsted, New York, 1986)
72. S.G. Samko, A.A. Kilbas, O.I. Marichev, *Fractional Integrals and Derivatives: Theory and Applications* (Gordon and Breach, Yverdon-les-Bains, 1993)
73. K. Nishimoto, *Fractional Calculus: Integrations and Differentiations of Arbitrary Order* (Univ. of New Haven Press, New Haven, 1989)
74. https://csrc.nist.gov/Projects/Random-Bit-Generation/Documentation-and-Software
75. Bassham III L. E., Rukhin A. L., Soto J., Nechvatal J. R., Smid M. E., Barker E. B., Leigh S., Levenson M., Vangel M., Banks D., Heckert A., Dray J., Vo S., NIST Sp 800-22 rev. 1a. A statistical test suite for random and pseudorandom number generators for cryptographic applications (2010)
76. D. Dua, C. Graff, UCI Machine Learning Repository [http://archive.ics.uci.edu/ml], University of California, School of Information and Computer Science, (Irvine, CA, 2019)
77. UCI Machine Learning Repository, https://archive.ics.uci.edu/ml/datasets/EEG+Eye+State#
78. J. Jezewski, A. Matonia, T. Kupka, D. Roj, R. Czabanski, Biomed Eng-Biomed Te. **57**, 5 (2012)